J. Fluid Mech. (2009), *vol.* 631, *pp.* 149–163.
doi:10.1017/S0022112009006788 Printed in the United Kingdom

Numerical study of vertical dispersion by stratified turbulence

G. BRETHOUWER† AND E. LINDBORG

Linné Flow Centre, Department of Mechanics, KTH, SE-100 44 Stockholm, Sweden

(Received 30 July 2008 and in revised form 19 February 2009)

Numerical simulations are carried out to investigate vertical fluid particle dispersion in uniformly stratified stationary turbulent flows. The results are compared with the analysis of Lindborg & Brethouwer (*J. Fluid Mech.*, vol. 614, 2008, pp. 303–314), who derived long- and short-time relations for the mean square vertical displacement $\langle \delta z^2 \rangle$ of fluid particles. Several direct numerical simulations (DNSs) with different degrees of stratification and different buoyancy Reynolds numbers are carried out to test the long-time relation $\langle \delta z^2 \rangle = 2\varepsilon_P t/N^2$. Here, ε_P is the mean dissipation of turbulent potential energy; N is the Brunt–Väisälä frequency; and t is time. The DNSs show good agreement with this relation, with a weak dependence on the buoyancy Reynolds number. Simulations with hyperviscosity are carried out to test the relation $\langle \delta z^2 \rangle = (1 + \pi C_{PL}) 2\varepsilon_P t/N^2$, which should be valid for shorter time scales in the range $N^{-1} \ll t \ll T$, where T is the turbulent eddy turnover time. The results of the hyperviscosity simulations come closer to this prediction with C_{PL} about 3 with increasing stratification. However, even in the simulation with the strongest stratification the growth of $\langle \delta z^2 \rangle$ is somewhat slower than linear in this regime. Based on the simulation results it is argued that the time scale determining the evolution of $\langle \delta z^2 \rangle$ is the eddy turnover time, T, rather than the buoyancy time scale N^{-1}, as suggested in previous studies. The simulation results are also consistent with the prediction of Lindborg & Brethouwer (2008) that the nearly flat plateau of $\langle \delta z^2 \rangle$ observed at $t \sim T$ should scale as $4E_P/N^2$, where E_P is the mean turbulent potential energy.

1. Introduction

Mixing of passive and active scalars in the atmosphere and oceans often occurs in stably stratified environments. Fluid particle dispersion studies in stratified flows can give insight into such processes and aid modelling efforts (Ivey, Winters & Koseff 2008). Lindborg & Brethouwer (2008; hereafter referred to as LB) derived long- and short-time relations for the vertical dispersion of fluid particles in stationary and decaying stratified turbulent flows. The analysis shows that the mean square of vertical particle displacements $\langle \delta z^2 \rangle$ for long times goes to a finite value in decaying turbulence, while in stationary flows it approaches $\langle \delta z^2 \rangle = (4E_P + 2\varepsilon_P t)/N^2$. Here E_P is the mean potential energy, ε_P the mean dissipation of potential energy and N the Brunt–Väisälä frequency. The first term in the relation represents the finite contribution of adiabatic dispersion, whereas the second term represents diabatic dispersion due to irreversible mixing. LB also suggested that for shorter time scales,

† Email address for correspondence: geert@mech.kth.se

between N^{-1} and T, there should be a range in which $\langle \delta z^2 \rangle = (1 + \pi C_{PL}) 2\varepsilon_P t/N^2$, where C_{PL} is a constant. Based on ocean observations by D'Asaro & Lien (2000) they made the estimate $C_{PL} \approx 3$. In this paper, we proceed the study of vertical particle dispersion in stationary stratified turbulent flows and compare results of numerical simulations with the relations derived by LB.

Vertical dispersion of particles in stationary stratified flows has previously been analysed by Pearson, Puttock & Hunt (1983). Using a Langevin model, they predicted a plateau with $\langle \delta z^2 \rangle \sim \langle w^2 \rangle / N^2$ (where w is the vertical velocity fluctuation), when the particle density does not change, and a linear growth $\langle \delta z^2 \rangle \sim \langle w^2 \rangle t/N$, when molecular diffusion alters the density of the particles. LB show that the latter result may be consistent with their relation for the diabatic dispersion. However, for the adiabatic dispersion the analysis by Pearson *et al.* (1983) and LB predict different results. In particular, Pearson *et al.* (1983) predicted that the asymptotic value of adiabatic dispersion is reached after $t \sim N^{-1}$, whereas according to the analysis by LB it is reached after a typical eddy turnover time and is independent of N.

Kaneda & Ishida (2000) analysed vertical dispersion in decaying stratified turbulence by applying rapid distortion theory together with Corrsin's conjecture. They predicted a plateau for $\langle \delta z^2 \rangle$ at long times which is consistent with direct numerical simulation (DNS) data and also with the result derived by LB. Nicolleau & Vassilicos (2000), Nicolleau & Yu (2007) and Nicolleau, Yu & Vassilicos (2008) studied dispersion in stationary rotating and stratified turbulence by kinematic simulations (KS). They observed $\langle \delta z^2 \rangle \sim E_K/N^2$ (E_K is mean kinetic energy) after long times. Diabatic dispersion was neglected because molecular diffusion is not included in KS. A linear model, KS and DNS were applied by Liechtenstein, Godeferd & Cambon (2005, 2006) to study dispersion in rotating and stratified turbulence. For decaying turbulence they found $\langle \delta z^2 \rangle \sim \langle w^2 \rangle / N^2$ after some time. A similar plateau was also observed in DNS of decaying stratified turbulence by Kimura & Herring (1996). The investigation by Venayagamoorthy & Stretch (2006) is one of few examining the role of diabatic particle displacements by changing particle density on vertical dispersion. Through DNS of decaying stratified turbulence, they found that adiabatic dispersion initially gives the largest contribution to vertical particle dispersion, but after about one eddy turnover time diabatic dispersion dominates. The analysis of LB is in agreement with this result. Simple models describing the latter process were then investigated by Venayagamoorthy & Stretch (2006). The first DNS study of particle dispersion in stationary stratified turbulence was by van Aartrijk, Clercx & Winters (2008). A plateau was observed with $\langle \delta z^2 \rangle \sim \langle w^2 \rangle / N^2$ after $t \sim N^{-1}$ but after longer times $\langle \delta z^2 \rangle \sim t$ in some of their simulations. The linear growth at late times, caused by density changes of fluid particles by molecular diffusion, can only be observed in stationary stratified flows as shown by LB. In the DNS by van Aartrijk *et al.* (2008) it was greatly reduced at higher Prandtl numbers. Such a reduction, however, is not to be expected in high-Reynolds-number flows if there is vigorous turbulent mixing down to the small scales (Venayagamoorthy & Stretch 2006). Although these studies have led to a better understanding of vertical dispersion in stratified flows there still remain questions about the quantitative contribution of adiabatic and diabatic dispersion.

Recent work on stratified flows can give useful background to dispersion studies. Lindborg (2006) examined strongly stratified turbulence and introduced the notion of elongated horizontal layers becoming unstable due to sharp vertical gradients and consequently breaking down into smaller structures. Those in turn, break down into even smaller structures and so on. Accordingly, an energy cascade from large to small

scales develops. This picture was consistent with numerical simulations of stratified turbulence by Lindborg (2006), Brethouwer *et al.* (2007) and Lindborg & Brethouwer (2007) who also observed an inertial range with $k_h^{-5/3}$ horizontal kinetic and potential energy spectra. The finding that strongly stratified flow dynamics, although very anisotropic, are essentially three-dimensional implies that even in this case turbulence contributes to vertical dispersion.

In this paper, we examine vertical particle dispersion in stationary and uniformly stratified turbulent flows through numerical simulations. The set-up of the simulations is similar to that of Lindborg (2006), Brethouwer *et al.* (2007) and Lindborg & Brethouwer (2007). The objective is to test the relations derived by LB and to clarify the role of adiabatic and diabatic dispersion on different time scales. The main steps and results of LB's analysis are recapitulated in the next section.

2. Analysis of vertical particle dispersion

Assuming a constant background stratification, the Boussinesq equations read

$$\frac{\mathrm{d}\boldsymbol{u}}{\mathrm{d}t} = -\frac{1}{\rho_0}\nabla p + \nu\nabla^2\boldsymbol{u} - Nb\boldsymbol{e}_z\,, \tag{2.1}$$

$$\nabla\cdot\boldsymbol{u} = 0\,, \tag{2.2}$$

$$\frac{\mathrm{d}b}{\mathrm{d}t} = \kappa\nabla^2 b + Nw\,. \tag{2.3}$$

Here, $\boldsymbol{u}$ is the velocity; w is the vertical velocity component; p is the pressure; ν and κ are the viscosity and diffusivity respectively; $\boldsymbol{e}_z$ is the unit vector in the vertical direction; N is the Brunt–Väisälä frequency; $b = g\rho'/(N\rho_0)$ with ρ' and ρ_0 the fluctuating and background density respectively; and g is the acceleration by gravity. With this buoyancy scaling the mean potential energy and the mean dissipation of potential energy per unit mass are respectively

$$E_P = \frac{1}{2}\langle b^2\rangle\,, \tag{2.4}$$

$$\varepsilon_P = \kappa\langle\nabla b\cdot\nabla b\rangle\,. \tag{2.5}$$

In this study, we consider homogeneous flows. After integrating (2.3) along a fluid particle trajectory and averaging over all fluid particles and some manipulations, we find (see LB for details)

$$\frac{\mathrm{d}\langle\delta z^2\rangle}{\mathrm{d}t} + \frac{2\kappa}{N}\int_0^t\langle\nabla^2 b(t')w(t)\rangle\,\mathrm{d}t' = \frac{2}{N^2}\left[\frac{\mathrm{d}E_P}{\mathrm{d}t} - \frac{\mathrm{d}\langle b(0)b(t)\rangle}{\mathrm{d}t} + \varepsilon_P + \kappa\langle b(0)\nabla^2 b(t)\rangle\right], \tag{2.6}$$

where $\delta z = z(t) - z(0)$, i.e. the vertical displacement of the fluid particle at time t with respect to its initial point of release. We can assume that the last term can be neglected for $t \gg \tau$, where τ is the Kolmogorov time scale.

The second term on the left-hand side of (2.6) needs some consideration because it cannot invariably be neglected in low- and moderate-Reynolds-number simulations. Pearson *et al.* (1983) argued that this term is a leading-order term, while other investigators (Pope 1998; Venayagamoorthy & Stretch 2006) have argued that it is small at high Reynolds numbers. In LB we argued that this term scales as $(\varepsilon_K\nu)^{1/2}$ for $t \gg \tau$, where ε_K is the dissipation rate of turbulent kinetic energy. Using this estimate

and integrating (2.6) for a statistically stationary flow, we obtain

$$\langle \delta z^2 \rangle = \frac{2}{N^2} \varepsilon_P t [1 - O(\mathscr{R}^{-1/2})] + \frac{\langle \delta b^2 \rangle}{N^2} \tag{2.7}$$

for $t \gg \tau$. Here $\delta b = b(t) - b(0)$ is the buoyancy change of a fluid particle and $\mathscr{R} = \varepsilon_K / \nu N^2$ is the buoyancy Reynolds number. The last term in (2.7) results from vertical isopycnal movements relative to their initial vertical positions. On longer time scales, this adiabatic dispersion is constrained by the available energy in the flow. The first term on the right-hand side of (2.7) results from density changes of the particles by molecular diffusion. Small-scale diapycnal mixing, strongly enhanced by turbulence, leads to irreversible changes of the equilibrium density levels about which the particles oscillate. The $O(\mathscr{R}^{-1/2})$ term may play an important role in mixing of stratified flow at low and moderate buoyancy Reynolds numbers.

For random initial conditions the adiabatic dispersion reaches the upper bound $4E_P/N^2$ as $t \to \infty$, and (2.7) becomes

$$\langle \delta z^2 \rangle = \frac{2}{N^2} [\varepsilon_P t (1 - O(\mathscr{R}^{-1/2})) + 2E_P]. \tag{2.8}$$

We expect (2.8) to be valid for $t \gg T$ in stratified turbulence, where T is an eddy turnover time.

In LB we assumed that stratified turbulence has an inertial range with a Lagrangian potential energy spectra of the form

$$E_{PL} = C_{PL} \varepsilon_P \omega^{-2} \tag{2.9}$$

for frequencies ω between T^{-1} and N. Here C_{PL} is a constant. From (2.9) we can deduce that the Lagrangian buoyancy structure function should have the form

$$\langle \delta b^2 \rangle = 2\pi C_{PL} \varepsilon_P t \tag{2.10}$$

for $N^{-1} \ll t \ll T$. Substituting this relation in (2.7) gives

$$\langle \delta z^2 \rangle = \frac{2}{N^2} \varepsilon_P t [1 + \pi C_{PL} - O(\mathscr{R}^{-1/2})]. \tag{2.11}$$

Using documented observations, LB estimated that $C_{PL} \simeq 3$. LB showed that (2.11) implies that the Lagrangian power spectrum of the vertical velocity is of the form

$$E_{wL} = \frac{2\varepsilon_P (1 + \pi C_{PL})}{\pi N^2} \tag{2.12}$$

for ω between T^{-1} and N. We expect relations (2.9)–(2.12) to be relevant to strongly stratified high-Reynolds-number flows.

In the next part of the paper we study vertical particle dispersion in stationary stratified turbulence through numerical simulations to test the suggested relations.

3. Numerical method

3.1. *Simulation of forced stratified turbulence*

We carry out a series of DNSs of homogeneous stratified turbulence. In addition, numerical simulations with hyperviscosity are carried out in order to study particle dispersion in stratified flows with a pronounced inertial range. The numerical method and codes are the same as in Brethouwer *et al.* (2007), Lindborg & Brethouwer (2007) and Brethouwer & Lindborg (2008). In the DNS, a pseudospectral approach

Run	Re ($\times 10^3$)	F_h	$\mathscr{R}$	Pr	L_h/L_v	$N_h \times N_v$	$k_{max}\eta$	E_P/E_K	$\varepsilon_P/\varepsilon_K$	$\langle w^2\rangle/2E_K$	Σ
A1	1.1	0.03	0.9	0.7	2.0	128×80	1.02	0.07	0.28	0.014	0.2
A2	2.1	0.02	0.9	0.7	3.3	256×96	1.03	0.08	0.29	0.011	0.2
A3	6.3	0.01	0.9	0.7	5.0	512×128	1.10	0.06	0.26	0.005	0.2
B1	1.0	0.1	9.3	0.7	2.0	128×80	1.06	0.18	0.51	0.11	3.4
B2	2.5	0.06	9.3	0.7	3.3	256×96	1.08	0.19	0.54	0.10	3.5
B3	5.5	0.04	9.5	0.7	5.0	512×128	1.15	0.17	0.51	0.07	3.4
B4	14	0.03	9.9	0.7	6.0	1024×256	1.21	0.15	0.48	0.06	3.4
C1	1.7	0.2	39	0.7	1.0	128×128	1.05	0.13	0.44	0.13	12
C2	2.8	0.11	37	0.7	1.0	256×256	1.08	0.16	0.54	0.13	14
C3	8.3	0.07	38	0.7	1.0	512×512	1.15	0.21	0.49	0.10	13
D1	1.3	2.2	6200	0.7	1.0	128×128	0.96	0.004	0.011	0.18	49
D2	2.4	1.6	6200	0.7	1.0	256×256	0.97	0.006	0.019	0.18	82
D3	8.9	0.8	5900	0.7	1.0	512×512	1.05	0.02	0.061	0.18	254
E1	1.0	0.2	44	2.8	1.0	256×256	2.05	0.14	0.30	0.14	36
E2	1.6	0.2	44	11.2	1.0	512×512	4.09	0.19	0.30	0.14	146

TABLE 1. Numerical and physical parameters of the DNSs: L_h/L_v is the aspect ratio of the horizontal to vertical domain size; N_h, N_v are the number of nodes in the horizontal and vertical direction respectively; k_{max} is the largest resolved horizontal wavenumber; $\Sigma = \varepsilon_P/\kappa N^2$ is the Cox number which is the ratio of the vertical eddy diffusivity to molecular diffusivity.

Run	F_h	L_h/L_v	$N_h \times N_v$	E_P/E_K	$\varepsilon_P/\varepsilon_K$	$\langle w^2\rangle/2E_K$	ν_h	ν_v
H1	0.0014	64	512×128	0.10	0.27	0.0006	1.05×10^{-15}	1.5×10^{-24}
H2	0.0008	72	768×256	0.11	0.28	0.0003	5.7×10^{-17}	4.2×10^{-27}
H3	0.0005	64	1024×512	0.13	0.29	0.0002	7.2×10^{-18}	6.5×10^{-29}

TABLE 2. Numerical and physical parameters of the hyperviscosity simulations.

with triple periodic boundary conditions is applied to solve the Boussinesq equations (2.1)–(2.3) with a constant background stratification. To obtain statistically stationary turbulence, we force the velocity field with a constant power input. Horizontal vortical modes are forced at horizontal wavenumbers $k_h \leqslant 3$. Since the flow is highly anisotropic in strongly stratified flows, we follow the approach taken by Brethouwer *et al.* (2007) and use computational domains stretched in the horizontal directions, taking care to resolve the largest vertical scales. In the simulations with hyperviscosity the same numerical approach is used, with the difference that the Laplacian diffusion operators in the integrated governing equations (2.1)–(2.3) are replaced by the operators

$$D_u = D_b = \nu_h \nabla_h^4 - \nu_v \frac{\partial^8}{\partial z^8}, \tag{3.1}$$

where ∇_h is the horizontal Laplace operator and ν_h and ν_v are horizontal and vertical diffusion coefficients respectively. More details on the numerical approach and forcing are found in Brethouwer *et al.* (2007) and Lindborg & Brethouwer (2007). Numerical and physical parameters of the DNSs and hyperviscosity simulations are presented in tables 1 and 2 respectively. In the DNS runs there are three independent non-dimensional parameters, the buoyancy Reynolds number, $\mathscr{R} = \varepsilon_K/(\nu N^2)$, the Froude number $F_h = \varepsilon_K/(N E_K)$, where E_K is the mean turbulent kinetic energy,

and the Prandtl number $Pr = \nu/\kappa$. The turbulent Reynolds number is defined as $Re = E_K^2/(\nu\varepsilon_K) = \mathscr{R}F_h^{-2}$. For $Pr \sim 1$, the resolution needed to carry out a DNS scales as $\mathscr{R}^{9/4}F_h^{-7/2}$. This means that it is very demanding to perform simulations with both large $\mathscr{R}$ and low F_h. With a fixed resolution we have to increase F_h when $\mathscr{R}$ is raised. First, four sets of simulations are carried out in which $\mathscr{R}$ is varied between the sets but is approximately equal for all simulations within each set, while F_h is varied. The value of Pr is equal to 0.7 in all these simulations. The four sets are designated A, B, C and D. Then, two DNSs, designated E1 and E2, are carried out with approximately the same $\mathscr{R}$ and F_h as in run C1 but with different Prandtl numbers. The resolution is successively doubled and the Prandtl number increased by a factor of four in runs E1 and E2, i.e. $Pr = 2.8$ and 11.2 respectively. In this way we ensure that the Batchelor scale $\eta/Pr^{1/2}$, with η the Kolmogorov length scale, is properly resolved. The Cox number Σ listed in table 1 is the ratio of the vertical eddy diffusivity, estimated as ε_P/N^2 in accordance with the analysis, and the molecular diffusivity. When the stratification is very strong, the Cox number is rather small, indicating a possible influence of Pr on the vertical dispersion. In the hyperviscosity simulations $\Delta z/l_O \simeq 7$ as in Lindborg & Brethouwer (2007), where $l_O = \varepsilon_K^{1/2}/N^{3/2}$ is the Ozmidov length scale and Δz the vertical grid spacing.

3.2. *Particle tracking*

To track fluid particles in the flow, we integrate

$$\frac{\mathrm{d}\boldsymbol{x}_p}{\mathrm{d}t} = \boldsymbol{u}_p \tag{3.2}$$

with a fourth-order Runge–Kutta scheme, using the same time step as in the simulation of the Eulerian field. To obtain the particle velocity $\boldsymbol{u}_p$ at the particle position $\boldsymbol{x}_p$, we employ a four-point Hermite interpolation scheme in the horizontal directions (Choi, Yeo & Lee 2004) and a direct summation of the Fourier modes in the vertical direction. When the flow is statistically stationary, we track 12 000–96 000 particles with a random initial distribution in the simulations. To obtain particle statistics, the DNSs are progressed till $t = 200\,T$ or even further ($T = E_P/\varepsilon_P$), except for runs B4, C3 and E2 which are progressed till $t = 100\,T$ or further.

4. Characteristics of the simulated flows

After an initial transition period, all simulations converge to a nearly statically stationary state in which the mean energy dissipation rate is equal to the imposed constant forcing power. In some runs, though, we observe a slow energy growth due to accumulation of energy in the shear mode, as also observed in some of our previous simulations, but this has a minor effect on particle dispersion statistics.

Brethouwer *et al.* (2007) discussed the importance of the horizontal Froude number, F_h, and the buoyancy Reynolds number, $\mathscr{R}$. A characteristic of strongly stratified flows with $F_h \ll 1$ is the horizontally layered structure with high shear rates between the layers (Riley & deBruynKops 2003). When $\mathscr{R} \lesssim 1$, vertical viscous shearing between the layers is strong and affects the dynamics. This can be seen in the snapshot of the buoyancy field taken from run A3 with $\mathscr{R} = 0.9$, shown in figure 1(*a*). Localized Kelvin–Helmholtz type of disturbances are present, but turbulence is suppressed, as is obvious from the smooth horizontal layers. Brethouwer *et al.* (2007) showed that when $\mathscr{R} \gg 1$ and $F_h \ll 1$ viscous forces are unimportant, and the vertical length scale l_v of the layers scales as $l_v \sim U/N$ (U is a characteristic horizontal velocity). The

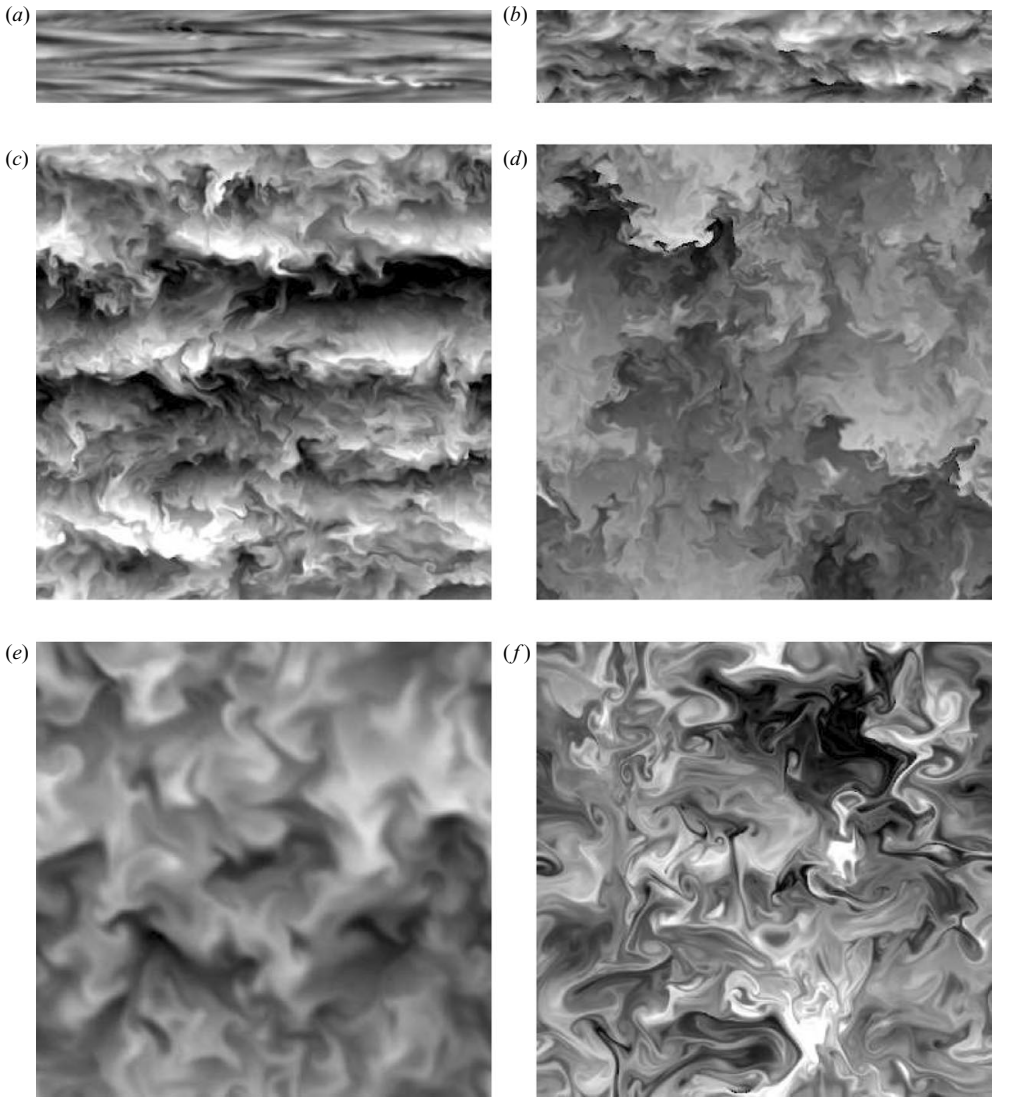

FIGURE 1. Snapshots of the buoyancy field in a vertical plane in runs (*a*) A3, (*b*) B3, (*c*) C3, (*d*) D3, (*e*) C1 and(*f*) E2.

horizontal layers are unstable and break down into smaller structures, giving rise to a three-dimensional but strongly anisotropic forward energy cascade. Snapshots of the buoyancy field in figure 1(*b*, *c*) taken from runs B3 and C3 show these features; a layered structure as well as turbulence can be observed. According to the scaling $l_v \sim U/N$ the thickness of the layers should be larger in run C3 than in run B3, which is also confirmed by the snapshots. The parameter $\mathscr{R}$ is proportional to $(l_O/\eta)^{4/3}$, where η the Kolmogorov length scale. This implies that there are two distinct ranges in strongly stratified turbulence when $\mathscr{R} \gg 1$. The dynamics of scales larger than l_O are strongly influenced by stratification and are anisotropic, while the dynamics at smaller scales are weakly influenced by stratification and approach isotropy at scales much smaller than l_O. For a comprehensive DNS study of the influence of $\mathscr{R}$ on spectra and energy transfer, please refer to Brethouwer *et al.* (2007). In most

geophysical flows $\mathscr{R} \gg 1$ and, consequently, stratified turbulence plays an important role in the oceans and atmosphere (Lindborg 2006; Lindborg & Brethouwer 2007; Brethouwer & Lindborg 2008). The layered structure and strong anisotropy disappear when $F_h \gtrsim 1$, as we see in the snapshot taken from run D3. Figure 1 also shows snapshots of the buoyancy field in runs C1 and E2 which have the same numerical set-up, except for the resolution and Pr. The flow is clearly turbulent in both runs, but as a result of a higher Pr, we see finer structures in run E2. The visualizations in figure 1 illustrate that we have simulated stratified flows with widely different dynamics.

5. Simulations versus analytical results

If $\mathscr{R} \gg 1$ the relations (2.8) and (2.11) can be written as

$$\langle \delta z^2 \rangle^* = 1 + \frac{1}{2} t^*, \quad t^* \gtrsim 1, \tag{5.1}$$

$$\langle \delta z^2 \rangle^* = \frac{1}{2} t^* (1 + \pi C_{PL}), \quad F_h \ll t^* \ll 1. \tag{5.2}$$

Here, $\langle \delta z^2 \rangle^* = \langle \delta z^2 \rangle N^2 / 4E_P$ and $t^* = t/T$ are the non-dimensional mean square of the vertical particle displacements and time respectively. For stratified turbulence, the eddy turnover time $T = E_P/\varepsilon_P$ can alternatively be estimated as E_K/ε_K.

5.1. *Vertical particle dispersion in DNS*

In figure 2 we show the time development of $\langle \delta z^2 \rangle^*$ versus t^* in the DNSs together with relations (5.1) and (5.2). DNSs with a similar value of $\mathscr{R}$ are grouped in the same plot. The initial period shows ballistic dispersion with $\langle \delta z^2 \rangle \sim t^2$ in all runs. Thereafter, the growth of $\langle \delta z^2 \rangle$ slows down. In the regime $F_h \ll t^* \ll 1$, (5.2) predicts $\langle \delta z^2 \rangle^* \sim t^*$. More generally, we expect that the evolution of $\langle \delta z^2 \rangle^*$ becomes independent of F_h when $R \gg 1$ and $F_h \ll 1$. In the B runs F_h is indeed small and $\mathscr{R}$ is quite large. Nevertheless, the curves in figure 2(*b*) still show a clear dependence on F_h for $t^* < 1$. The mean square displacement, $\langle \delta z^2 \rangle^*$, moves closer to the straight line representing (5.2) as F_h decreases, but no linear range is visible. We must conclude that we have to perform simulations with considerably lower F_h in order to test the relation (5.2). Unfortunately, this is not possible using DNS.

In the simulations with $F_h < 1$ we see the onset of a plateau at $t^* \sim 1$, as expected. This is most clearly seen in figure 2(*b*). It resembles the plateau observed by van Aartrijk *et al.* (2008) and indicates that the adiabatic mean square displacement has approached its upper bound $\langle \delta z^2 \rangle = 4E_P/N^2$, i.e. $\langle \delta z^2 \rangle^* = 1$. According to the analysis of LB, the onset of the plateau shows up at $t^* \lesssim 1$, while diabatic dispersion begins to dominate at $t^* \simeq 2$. The time scale separation is thus not very large, and consequently an extended plateau will not appear in stationary flows as long as $\mathscr{R} \gtrsim 1$. However, this might be different when $\mathscr{R} \ll 1$. Van Aartrijk *et al.* (2008) obtained in the latter case a long plateau in their DNS. The adiabatic dispersion regime or the onset of a plateau cannot be seen in DNS results with $F_h \gtrsim 1$ displayed in figure 2(*d*). Van Aartrijk *et al.* (2008) observed the same behaviour.

After the slowdown of vertical dispersion seen in figure 2(*a–c*), $\langle \delta z^2 \rangle^*$ grows faster again and approaches the asymptotic diabatic dispersion limit (5.1) with $\langle \delta z^2 \rangle^* \sim t^*$. The DNS data displayed in figure 2 nicely approach this limit. Noticeable is that the asymptotic diabatic dispersion limit is seen in all our DNSs with strong as well as weak stratification with a difference in F_h of about two orders of magnitude. Furthermore,

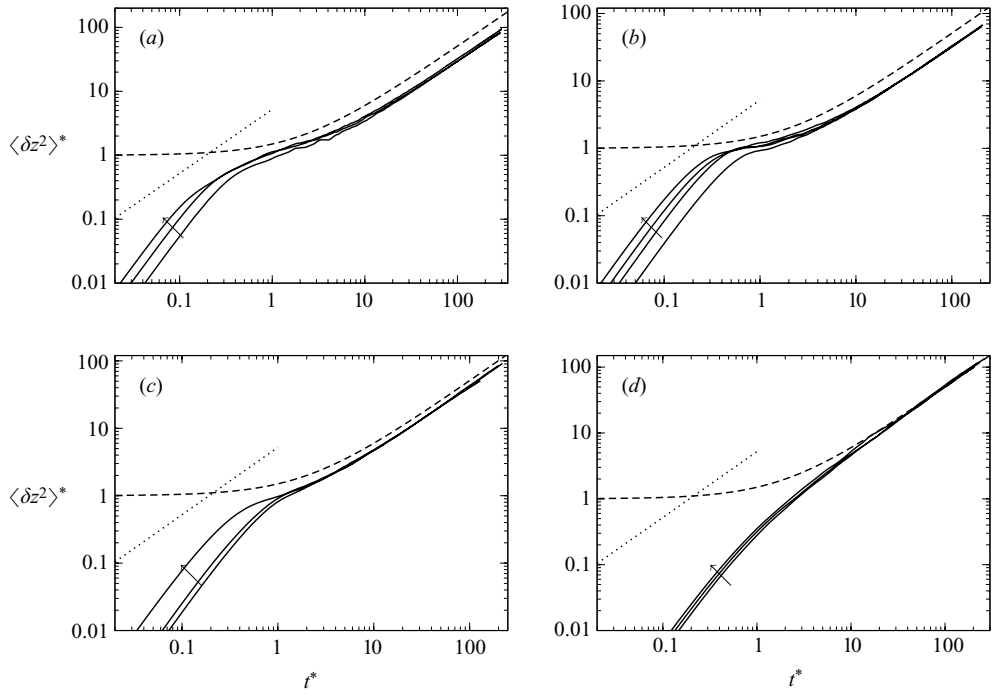

FIGURE 2. Time development of $\langle \delta z^2 \rangle^*$ versus t^*. The dashed and dotted lines show relations (5.1) and (5.2) respectively, and the solid lines show DNS results. The arrow indicates the direction of decreasing F_h or increasing Re. (*a*) A runs ($\mathscr{R} \simeq 1$), (*b*) B runs ($\mathscr{R} \simeq 9$), (*c*) C runs ($\mathscr{R} \simeq 38$), (*d*) D runs ($\mathscr{R} \simeq 6000$).

the plots show the collapse of $\langle \delta z^2 \rangle^*$ for $t^* > 1$ in DNSs with approximately equal $\mathscr{R}$. The buoyancy Reynolds number, $\mathscr{R}$, is successively increased as we go from the A runs in figure 2(*a*) to the D runs in figure 2(*d*). The relation (2.7) predicts that $\langle \delta z^2 \rangle^* \to t^*/2$ for long times, as $\mathscr{R}$ is increased. Going from figure 2(*a*) to figure 2(*d*) we see that the simulation results are consistent with this prediction. Note that the linear growth at late times only can be observed in stationary flows as explained by LB. In decaying stratified turbulence, $\langle \delta z^2 \rangle$ goes to a constant as observed in many DNSs (Kimura & Herring 1996; Kaneda & Ishida 2000; Venayagamoorthy & Stretch 2006). We have also confirmed this in simulations that are not presented here.

Figure 3 shows the time development of $\langle \delta z^2 \rangle^*$ versus t^* in runs C1, E1 and E2. These DNSs have the same numerical set-up, except for the resolution and Pr which is 0.7, 2.8 and 11.2 in runs C1, E1 and E2 respectively. When Re is sufficiently high we can expect molecular diffusivity to have a small influence on the dispersion of particles (Venayagamoorthy & Stretch 2006). In figure 3 we see little difference between the runs in the late-time dispersion, but ε_P is somewhat smaller for $Pr > 1$ than for $Pr < 1$ as shown in table 1, implying that the vertical diapycnal dispersion is slightly smaller in runs E1 and E2 than in run C. Overall the influence of Pr are relatively small if $\mathscr{R} \gg 1$, which illustrates the turbulent nature of the diabatic dispersion. In contrast, diabatic dispersion reduces strongly for increasing Pr in our DNS when $\mathscr{R} < 1$ and when small-scale turbulent mixing is mostly absent (results not presented here). This was already shown by van Aartrijk *et al.* (2008). Since $\langle \delta z^2 \rangle$ approaches the asymptote $2\varepsilon_P t/N^2$ in all DNSs, we can firmly conclude that diabatic

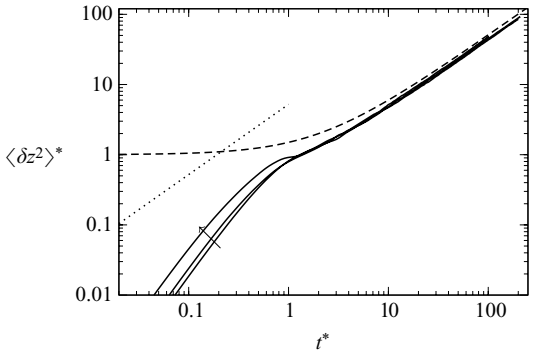

FIGURE 3. Time development of $\langle \delta z^2 \rangle^*$ versus t^*. The dashed and dotted lines show relations (5.1) and (5.2) respectively, and the solid lines show results of runs C1, E1 and E2. The arrow indicates the direction of increasing Pr.

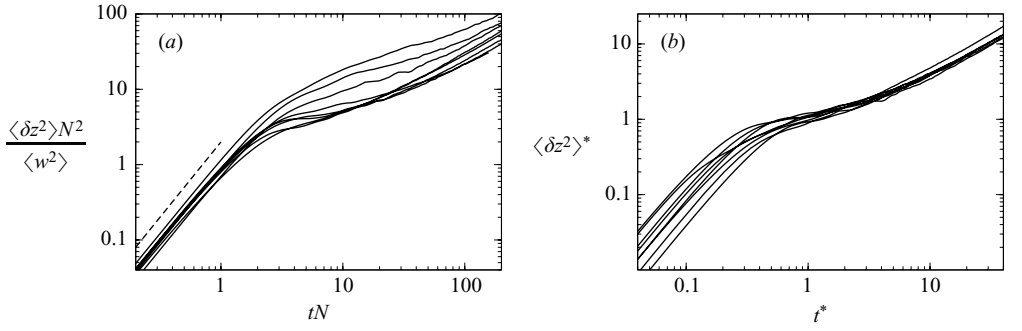

FIGURE 4. (*a*) Time development of $\langle \delta z^2 \rangle N^2 / \langle w^2 \rangle$ versus tN; (*b*) $\langle \delta z^2 \rangle^*$ versus t^*. The solid lines are the results of all A and B runs and run C3. The dashed line in (*a*) indicates $\langle \delta z^2 \rangle \sim t^2$.

dispersion determines mixing of weakly and strongly stratified flows with different Reynolds and Prandtl numbers.

In figure 4(*a*) we have collected most of the DNS data to focus on the initial dispersion stage. All runs initially display ballistic dispersion with $\langle \delta z^2 \rangle \approx \langle w^2 \rangle t^2$. If $\langle w^2 \rangle$ had been calculated as a Lagrangian mean value over the initial field we would have $\langle \delta z^2 \rangle = \langle w^2 \rangle t^2$, exactly. Here, we have instead calculated $\langle w^2 \rangle$ as a space–time mean value over a whole simulation, and therefore this relation is only approximately satisfied. Pearson *et al.* (1983) suggested that the adiabatic dispersion should be bounded by $\langle \delta z^2 \rangle \simeq \langle w^2 \rangle / N^2$ and reach this limit at $t \simeq N^{-1}$. This behaviour was observed by van Aartrijk *et al.* (2008) in their DNS. In our DNS, scaling of $\langle \delta z^2 \rangle$ and t by $\langle w^2 \rangle / N^2$ and N^{-1} respectively does not lead to a collapse of the onset of the adiabatic dispersion plateau in the many DNSs, as we see in figure 4(*a*). The reason why we do not observe this scaling is that our DNS covers the regime $\mathscr{R} \gtrsim 1$, while van Aartrijk *et al.* (2008) considered the regime $\mathscr{R} \lesssim 1$. Figure 4(*b*) shows the time development of $\langle \delta z^2 \rangle^*$ versus t^* for the same runs. Indeed, the onset of the adiabatic dispersion plateau appears when $\langle \delta z^2 \rangle \simeq 4E_P / N^2$, in accordance with (5.1), rather than $\langle \delta z^2 \rangle \simeq \langle w^2 \rangle / N^2$. The range of F_h is too limited to firmly determine whether the onset appears when $t \sim E_P / \varepsilon_P$ ($t^* \sim 1$) or when $t \propto N^{-1}$ as suggested by LB and Pearson *et al.* (1983) respectively. Nevertheless, comparing the onset of the adiabatic dispersion plateaus in figure 4, we see that the DNS data are in better agreement

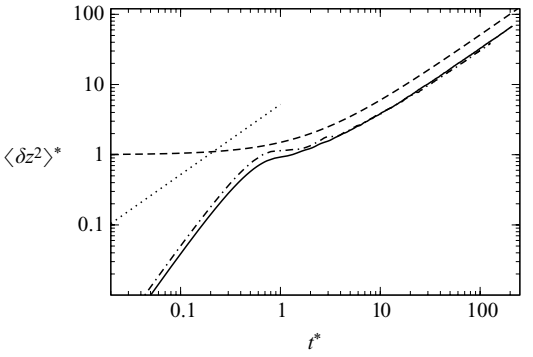

FIGURE 5. Time development of $\langle \delta z^2 \rangle^*$ vesus t^*. The dashed and dotted lines show relations (5.1) and (5.2) respectively; the solid and dash-dotted lines are the result of DNSs with vortical forcing (run B1) and wave forcing ($\mathscr{R} \approx 10$) respectively.

with LB's suggestion. Venayagamoorthy & Stretch (2006) also found that T is the relevant dispersion time scale, rather than N^{-1}.

In order to illustrate the relative independence of the results from the forcing methodology, we show in figure 5 the dispersion results of DNS with vortical forcing and wave forcing. The forcing method we used in each case is described in Lindborg & Brethouwer (2007). Both simulations reveal the same asymptotic dispersion behaviour, while for shorter times the differences are only small. However, this independence does probably only exist for $\mathscr{R} > 1$. Van Aartrijk *et al.* (2008) observed that the growth of $\langle \delta z^2 \rangle$ was dependent on the forcing method in the regime $\mathscr{R} < 1$. The independence that we observed here for $\mathscr{R} > 1$ is consistent with Lindborg & Brethouwer (2007) who found that stratified turbulence dynamics are similar in simulations with vortical forcing and simulations with wave forcing if the vertical forcing wavenumber is sufficiently large.

5.2. *Adiabatic dispersion in hyperviscosity simulations*

Since the DNSs do not reveal a clear inertial stratified turbulence range and prohibit a detailed investigation of adiabatic dispersion, we have carried out additional hyperviscosity simulations in order to test the relations suggested by LB. Stratified turbulence features in hyperviscosity simulations, having a well-defined inertial range, have extensively been examined by Lindborg (2006), Lindborg & Brethouwer (2007) and Brethouwer & Lindborg (2008). The numerical approach here is the same as in those studies, and therefore we refer the reader to those studies for the Eulerian spectra. The inertial range seen in the horizontal Eulerian spectra is the result of stratified turbulence and not Kolmogorov turbulence because it occurs at scales larger than l_O. Here, we look for inertial features in the Lagrangian statistics extracted from the particles. Figure 6(a) shows the Lagrangian frequency spectrum of the buoyancy fluctuations. At frequencies lower than N there is a narrow range of scales where the Lagrangian buoyancy spectra are not far from displaying an inertial range in accordance with (2.9), with $C_{PL} \approx 3$. We must note that in the hyperviscosity simulations we do not resolve the motions down to the Ozmidov length scale, l_O. Consequently, we cannot deduce the higher cutoff frequency of (2.9) from the simulations, but it indicates that it is at least $O(N)$. In the same range of frequencies we can expect the Lagrangian spectrum of the vertical velocity fluctuations to have the form (2.12). This spectrum is shown in figure 6(b). For the same frequencies as

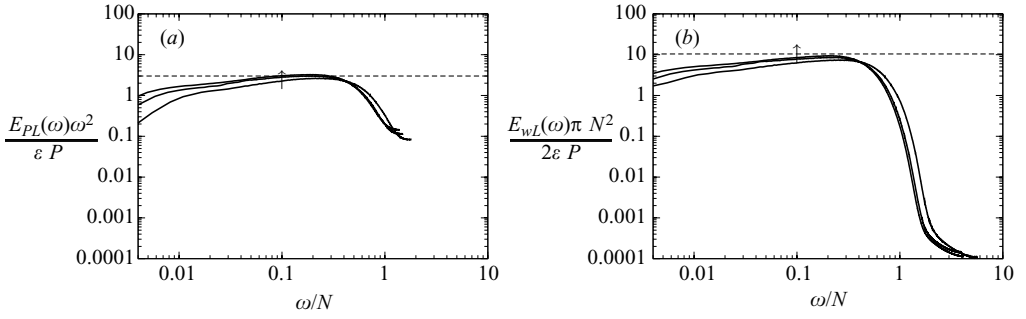

FIGURE 6. (*a*) Compensated Lagrangian frequency spectrum of the buoyancy $E_{PL}(\omega)\omega^2/\varepsilon_P$. The straight dashed line is $C_{PL}=3$. (*b*) Lagrangian frequency spectrum of the vertical velocity fluctuations $E_{wL}(\omega)\pi N^2/2\varepsilon_P$. The straight dashed line is $1+\pi C_{PL}$ with $C_{PL}=3$. In both plots the solid lines show the result of the hyperviscosity simulations. The arrow indicates the direction of decreasing F_h.

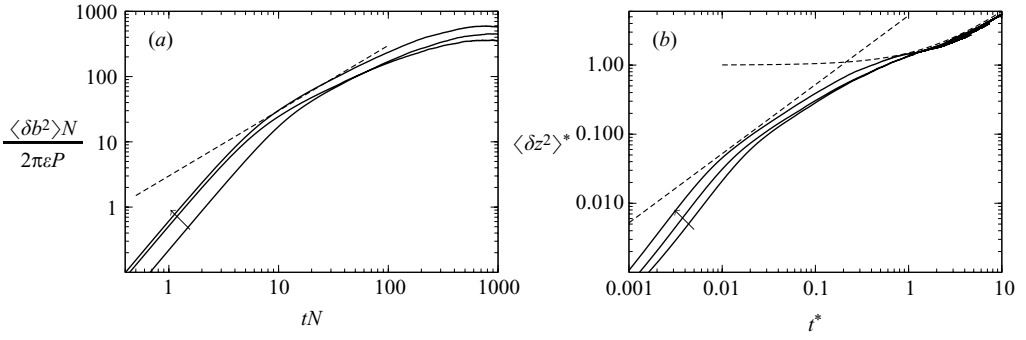

FIGURE 7. (*a*) Lagrangian buoyancy structure function $\langle\delta b^2\rangle N/2\pi\varepsilon_P$. The straight dashed line is $\langle\delta b^2\rangle = 2\pi C_{PL}\varepsilon_P t$. (*b*) Time development of $\langle\delta z^2\rangle^*$ versus t^*. The straight and bent thin dashed lines show relations (5.2) and (5.1) respectively. In both plots the solid lines show the result of the hyperviscosity simulations. The arrow indicates the direction of decreasing F_h.

in figure 6(*a*) we see, indeed, a narrow inertial range approaching (2.12) and $C_{PL}\approx 3$. D'Asaro & Lien (2000) measured the power spectrum of the vertical velocity in the ocean's thermocline and observed a flat spectrum till $\omega\simeq N$, in agreement with (2.12) and our simulations.

Since the Lagrangian buoyancy spectrum approaches (2.9), the Lagrangian structure function of the buoyancy should approximate (2.10). This structure function is displayed in figure 7(*a*). For short times corresponding to the ballistic regime $\langle\delta b^2\rangle\sim t^2$, while for $t>N^{-1}$ there is a limited range of scales in the hyperviscosity simulations in which $\langle\delta b^2\rangle$ moves closer to relation (2.10) with $C_{PL}=3$ when F_h becomes smaller, but there is no obvious inertial range. At longer times $\langle\delta b^2\rangle$ levels off and approaches its upper adiabatic dispersion bound $4E_P$.

Figure 7(*b*) shows the time development of $\langle\delta z^2\rangle^*$ in the hyperviscosity simulations together with relations (5.1) and (5.2). Also in the hyperviscosity simulations, $\langle\delta z^2\rangle^*$ approaches the diabatic dispersion asymptote (5.1) at long times. The small differences are owing to the small-scale anisotropy in the simulations, a consequence of the different diffusivities in the horizontal and vertical directions, and the truncation of the inertial range at a scale larger than l_O. For increasing stratification, $\langle\delta z^2\rangle$ moves

closer to expression (5.2) for the adiabatic dispersion in the inertial range of stratified turbulence with $C_{PL} = 3$ for $N^{-1} \ll t \ll T$, but there is no extended range in which it matches the relation. We can only speculate that it may require very extended inertial ranges as in geophysical flows to observe the behaviour expressed by (5.2). The numerical results shown in figures 6 and 7 indicate that C_{PL} is between 2 and 4, which is quite close to the estimation made by LB.

6. Conclusions

We have used forced DNSs and numerical simulations with hyperviscosity to examine vertical fluid particle dispersion in stationary and uniformly stratified turbulent flows. The simulation results are in good agreement with relation (2.8) for the mean square of the vertical fluid displacements, $\langle \delta z^2 \rangle$, derived by LB. For increasing stratification the adiabatic dispersion contribution, represented by the second term on the right-hand side of (2.7), moves closer to LB's suggestion $2\pi C_{PL} \varepsilon_P t/N^2$ with $C_{PL} \sim 3$ for $N^{-1} \ll t \ll T$, according to the simulations with hyperviscosity. However, the growth of $\langle \delta z^2 \rangle$ is somewhat slower than linear even in the simulation with the strongest stratification. Structure functions and power spectra of the buoyancy show reasonable consistency with or seem to approach the proposed relations by LB. At about $t \approx T$ we see the onset of a plateau, since the adiabatic dispersion reaches its upper bound $4E_P/N^2$. The last term, $2\varepsilon_P t/N^2$, in the relation derived by LB represents diabatic dispersion. In all our simulations, spanning quite an extended range of Froude and Reynolds numbers, $\langle \delta z^2 \rangle$ approaches $2\varepsilon_P t/N^2$ in the long-time limit. This linear growth allows us to define the eddy diffusivity in a way which is analogous to the definition of molecular diffusivity. According to the analysis of Einstein (1956), the molecular diffusivity can be defined from the growth of the mean square displacement of molecules. Analogously, the linear growth of the vertical mean square displacement of fluid particles suggests that the vertical eddy diffusivity of stratified turbulence can be calculated as

$$K_{\mathscr{E}} = \frac{1}{2} \frac{\mathrm{d}}{\mathrm{d}t} \langle \delta z^2 \rangle = \frac{\varepsilon_P}{N^2} \tag{6.1}$$

in the long-time limit. The expression (6.1) is equivalent to Osborn's (1980) expression $\Gamma \varepsilon_K / N^2$ for the eddy diffusivity for buoyancy, where $\Gamma = \varepsilon_P / \varepsilon_K$ is the flux coefficient, sometimes referred to as the 'mixing efficiency'. Osborn (1980) derived this expression using similar arguments as Osborn & Cox (1972), who derived a corresponding expression for the eddy diffusivity for temperature. The main assumption of Osborn & Cox (1972) is that there is an approximate balance between production and dissipation in the governing equation for the scalar variance. In the analysis of Osborn & Cox (1972) the scalar is temperature, and in the analysis of Osborn (1980) the scalar is buoyancy. As shown by Winters & D'Asaro (1996) the balance assumption leads to different eddy diffusivities for different scalars, each depending on the mean gradient of the particular scalar which is being diffused. As pointed out by Lindborg & Fedina (2009), the statistical mechanical argument which is the basis for the expression (6.1), on the other hand, suggests that this expression is the eddy diffusivity for any scalar which is following fluid particles. In simulations of the Boussinesq equations with hyperviscosity, together with the equation for a freely diffusing passive scalar, Lindborg & Fedina (2009) showed that the vertical turbulent diffusion of a passive scalar is very well described by the classical diffusion equation with an associated eddy diffusivity given by (6.1).

The vertical eddy diffusivity is a quantity of great practical importance in oceanography as well as meteorology. The numerical verification of the linear growth of $\langle \delta z^2 \rangle$ which we have presented in this paper may therefore be a result which can influence these fields.

We acknowledge financial support from the Swedish Research Council. Computational resources at PDC were made available by the Swedish National Infrastructure for Computing.

REFERENCES

van Aartrijk, M., Clercx, H. J. H. & Winters, K. B. 2008 Single-particle, particle-pair, and multiparticle dispersion of fluid particles in forced stably stratified turbulence. *Phys. Fluids* **20**, 025104.

Brethouwer, G., Billant, P., Lindborg, E. & Chomaz, J.-M. 2007 Scaling analysis and simulation of strongly stratified turbulent flows. *J. Fluid Mech.* **585**, 343–368.

Brethouwer, G. & Lindborg, E. 2008 Passive scalars in stratified turbulence. *Geophys. Res. Lett.* **35**, L06809.

Choi, J.-I., Yeo, K. & Lee, C. 2004 Lagrangian statistics in turbulent channel flow. *Phys. Fluids* **16**, 779–793.

D'Asaro, E. A. & Lien, R.-C. 2000 Lagrangian measurements of waves and turbulence in stratified flows. *J. Phys. Oceanogr.* **30**, 641–654.

Einstein, A. 1956 On the movement of small particles suspended in a stationary liquid demanded by the molecular-kinetic theory of heat. In *Investigations on the Theory of the Brownian Movement* (ed. F. Fürth). Dover. Pp. 1–17.

Ivey, G. N., Winters, K. B. & Koseff, J. R. 2008 Density stratification, turbulence, but how much mixing? *Annu. Rev. Fluid Mech.* **40**, 169–184.

Kaneda, Y. & Ishida, T. 2000 Suppression of vertical diffusion in strongly stratified turbulence. *J. Fluid Mech.* **402**, 311–327.

Kimura, Y. & Herring, J. R. 1996 Diffusion in stably stratified turbulence. *J. Fluid Mech.* **328**, 253–269.

Liechtenstein, L., Godeferd, F. S. & Cambon, C. 2005 Nonlinear formation of structures in rotating stratified turbulence. *J. Turbul.* **6**, 1–18.

Liechtenstein, L., Godeferd, F. S. & Cambon, C. 2006 The role of nonlinearity in turbulent diffusion models for stably stratified and rotating turbulence. *Intl J. Heat Fluid Flow* **27**, 644–652.

Lindborg, E. 2006 The energy cascade in a strongly stratified fluid. *J. Fluid Mech.* **550**, 207–242.

Lindborg, E. & Brethouwer, G. 2007 Stratified turbulence forced in rotational and divergent modes. *J. Fluid Mech.* **586**, 83–108.

Lindborg, E. & Brethouwer, G. 2008 Vertical dispersion by stratified turbulence. *J. Fluid Mech.* **614**, 303–314.

Lindborg, E. & Fedina, E. 2009 Vertical turbulent diffusion in stably stratified flows. *Geophys. Res. Lett.* **36**, L01605.

Nicolleau, F. & Vassilicos, J. C. 2000 Turbulent diffusion in stably stratified non-decaying turbulence. *J. Fluid Mech.* **410**, 123–146.

Nicolleau, F. & Yu, G. 2007 Turbulence with combined stratification and rotation: limitations of Corrsin's hypothesis. *Phys. Rev.* E **76**, 066302.

Nicolleau, F., Yu, G. & Vassilicos, J. C. 2008 Kinematic simulation for stably stratified and rotating turbulence. *Fluid Dyn. Res.* **40**, 68–93.

Osborn, T. R. 1980 Estimates of the local rate of vertical diffusion from dissipation measurements. *J. Phys. Oceanogr.* **10**, 83–89.

Osborn, T. R. & Cox, C. S. 1972 Oceanic fine structure. *Geophys. Fluid Dyn.* **3**, 321–345.

Pearson, H. J., Puttock, J. S. & Hunt, J. C. R. 1983 A statistical model of fluid-element motions and vertical diffusion in a homogeneous stratified turbulent flow. *J. Fluid Mech.* **129**, 219–249.

Pope, S. B. 1998 The vanishing effect of molecular diffusivity on turbulent dispersion: implications for turbulent mixing and the scalar flux. *J. Fluid Mech.* **359**, 299–312.

Riley, J. J. & deBruynKops, S. M. 2003 Dynamics of turbulence strongly influenced by buoyancy. *Phys. Fluids* **15**, 2047–2059.

Venayagamoorthy, S. K. & Stretch, D. D. 2006 Lagrangian mixing in decaying stably stratified turbulence. *J. Fluid Mech.* **564**, 197–226.

Winters, K. B. & D'Asaro, E. A. 1996 Diascalar flux and the rate of fluid mixing. *J. Fluid Mech.* **317**, 179–193.